Model for binary alloys: An Ising model with isotropic competing interactions

Paul Upton
Institute for Physical Science and Technology, University of Maryland, College Park, Maryland 20742

Julia Yeomans
Department of Theoretical Physics, 1 Keble Road, Oxford, OX1 3NP, England

(Received 23 January 1989)

An Ising model with competing interactions isotropic with respect to the cubic axes is presented as a model for binary alloys exhibiting modulated structural order. In the mean-field approximation the model supports incommensurate and commensurate structures with modulation in one, two, and three lattice directions. The behavior of the model near a "superdegenerate" point, where the zero-temperature entropy per spin is nonvanishing, is discussed, and low-temperature series are employed to distinguish between modulated phases which have the same mean-field free energy.

I. INTRODUCTION

Models with competing interactions that result in modulated commensurate and incommensurate phases have received considerable attention recently.[1–3] Not only are they of theoretical interest, but they seem relevant to a surprisingly large number of experimental systems such as binary alloys, polytypes, and ferrimagnets.[2]

One of the most interesting cases of structural modulation that has been observed is in binary alloys of the AB_3 type such as $TiAl_3$ (Ref. 4) and Cu_3Pd.[5] These order in the Ll_2 structure shown in Fig. 1(a). Modulation then manifests itself through regular arrays of antiphase boundaries as shown in Fig. 1(b). One can represent the long-period superstructures of these alloys using a spin representation. Each structural unit is depicted by an up (+) or down (−) spin depending on its position as shown by the example in Fig. 1(b). Long-period superstructures then correspond to repeating sequences of bands of spins.

Kulik and de Fontaine[6,4] have proposed that the spins, representing the two positions occupied by the structural units, interact through the Hamiltonian of the axial next-nearest-neighbor Ising, (ANNNI) model.[7–9] This model has competing first- and second-neighbor interactions in one axial direction leading to an infinite number of modulated phases which bear a strong resemblance to those observed in many binary alloys.

Although this appears to provide a possible explanation of the existence of long-period superstructures, one is still left with some unanswered questions. One problem is that the interactions of the ANNNI model are anisotropic. In the absence of strain, one would expect the couplings between the structural units of the binary alloys to be isotropic with respect to the cubic-lattice directions; there is no reason to expect a preferred axis as in the ANNNI model. Moreover, the ANNNI model cannot explain the existence of phases modulated in more than one lattice direction. Such structures have been observed in binary alloys.[10,5]

As a first attempt to remedy these defects, in this paper we introduce an Ising model with isotropic competing interactions. It is found that the model supports not only the commensurate and incommensurate states found in the ANNNI model, but also phases modulated in more than one lattice direction. Moreover, the model proves to be of considerable theoretical interest in its own right. Related models have been applied to the study of microemulsions[11–13] and similar two-dimensional models have been considered.[14–16]

We start by defining the model and describing its rather complicated ground states in Sec. II. One interesting degeneracy in the ground state occurs between states or-

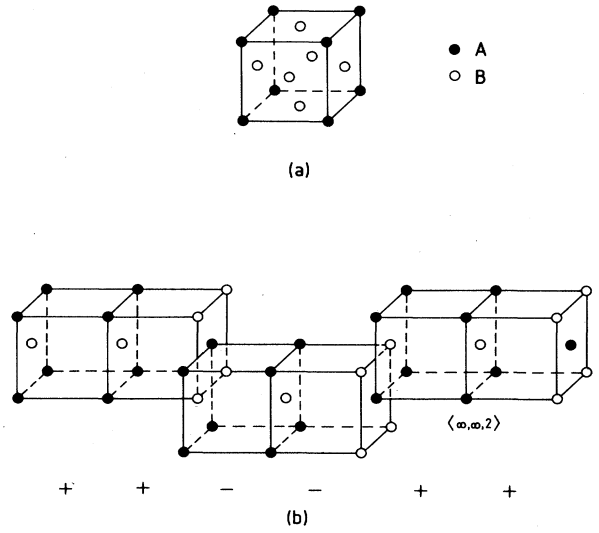

FIG. 1. Atomic arrangement of the binary alloy AB_3 showing (a) the Ll_2 structure and (b) the $\langle \infty, \infty, 2 \rangle$ phase. Intervening planes composed entirely of B atoms have been omitted for clarity.

dered like a chessboard and those ordered like a staircase. In Sec. III we show, using low-temperature series expansions, how this degeneracy is broken at finite temperature. This problem has also been studied in the two-dimensional model.[14–16]

The mean-field theory for the model is described in Sec. IV which uses methods originally developed for the ANNNI model.[9,17] Indeed, we show that much of the mean-field phase diagram at low temperatures can be understood through a mapping to the coupling constants of the ANNNI model.[11] The phase diagram near the order-disorder transition surface is obtained and compared to that at low temperatures. Some predictions on the ordering near this transition can be obtained through a Landau theory of the type used to study Lifshitz points. Explanation of this is left to the Appendix.

An interesting feature of the model is that it contains a "superdegenerate" point where the degeneracy of the ground state is so high that there is a nonzero entropy per spin at zero temperature. These ground states contain fully frustrated spins which can flip without any change in energy. Effects due to this situation are discussed in Sec. V.

The paper is concluded with a discussion of outstanding theoretical questions, both with regard to the analysis of the model and its relevance to ordering in binary alloys. A brief account of some of the ideas presented here has been published elsewhere.[18]

II. THE MODEL AND ITS GROUND STATES

Ising spins, $S_{\mathbf{r}}$, are placed on the sites, $\mathbf{r}$, of a cubic lattice and interact through the Hamiltonian

$$\mathcal{H}\{S\}=-\frac{1}{2}\sum_{\mathbf{r},\mathbf{r}'}\mathcal{J}(\mathbf{r}-\mathbf{r}')S_{\mathbf{r}}S_{\mathbf{r}'},\quad S_{\mathbf{r}}=\pm 1,\quad \mathbf{r}\in\mathbb{Z}^3\ , \tag{2.1}$$

where the coupling constant is given by

$$\mathcal{J}(\mathbf{r}-\mathbf{r}')=\begin{cases} J, & \text{between nearest-neighbor sites}\\ -\kappa_1|J|, & \text{between next-nearest-neighbor}\\ & \text{sites along cubic axes}\\ -\kappa_2|J|, & \text{between next-nearest-neighbor}\\ & \text{sites across face diagonals}\end{cases} \tag{2.2}$$

and the interactions between all other spins are taken to be zero.

The ground states of this model can be determined using the cluster method of Lyons and Kaplan.[19] One starts by dividing the lattice into octahedral clusters of seven spins as shown in Fig. 2(a). For convenience we use the planar representation illustrated in Fig. 2(b). The couplings between spins on a cluster are shown in Fig. 3. They are weighted according to how many times the bonds are counted when adding up all the clusters on the lattice. In this way, the sum of the energies of all the individual clusters that make up the entire lattice state will give the total ground-state energy.

It is readily seen from Fig. 3 that the Hamiltonian (2.1) has a simple symmetry property. This states that under the transformation $J\rightarrow -J$ the ground-state energy is unchanged provided $S_{\mathbf{r}}\rightarrow -S_{\mathbf{r}}$ for the central spin of every nonoverlapping cluster. In other words, the phase diagram is symmetric about $J=0$, and if the phases for $J>0$

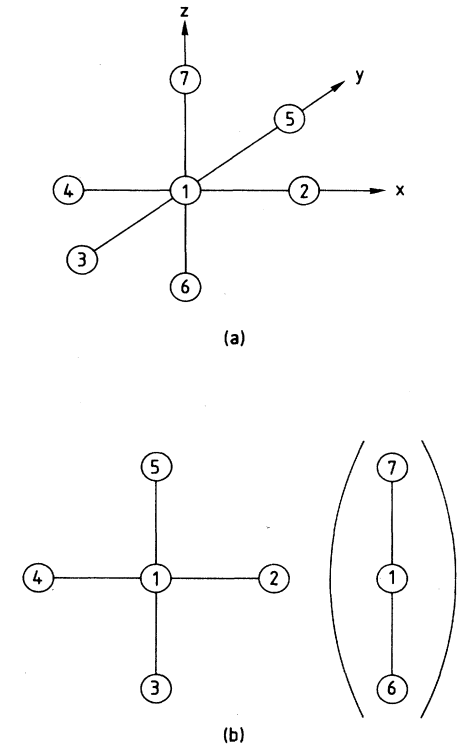

FIG. 2. (a) The octahedral cluster used for determining the ground state of the Hamiltonian (2.1). (b) Its planar representation.

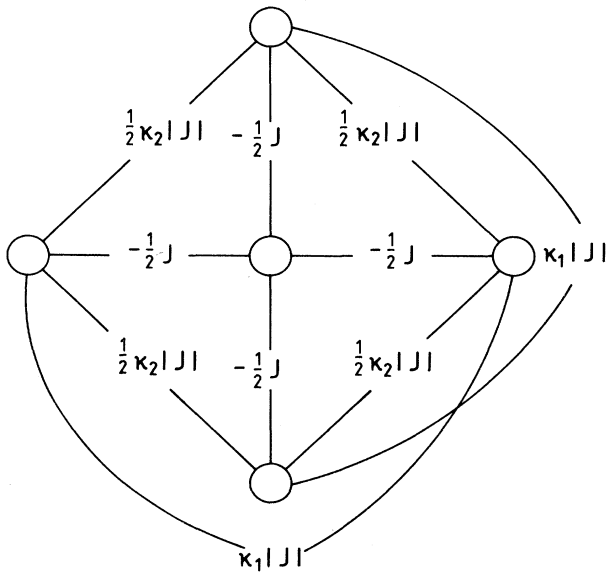

FIG. 3. Assignment of couplings between coplanar sites of a cluster. Couplings to the other two sites are omitted for clarity.

TABLE I. The ten distinct configurations a cluster state can take. In calculating the cluster energies, it was assumed that $J > 0$.

Cluster state	Degeneracy	Cluster energy/J	Lattice state
$\begin{matrix} & + & \\ + & + & + \\ & + & \end{matrix}$ $\begin{bmatrix} + \\ + \\ + \end{bmatrix}$	2	$-3+3\kappa_1+6\kappa_2$	$\langle \infty,\infty,\infty \rangle$
$\begin{matrix} & + & \\ + & + & + \\ & + & \end{matrix}$ $\begin{bmatrix} + \\ + \\ - \end{bmatrix}$	12	$-2+\kappa_1+2\kappa_2$	$\langle \infty,\infty,2 \rangle$
$\begin{matrix} & + & \\ + & + & + \\ & + & \end{matrix}$ $\begin{bmatrix} - \\ + \\ - \end{bmatrix}$	6	$-1+3\kappa_1-2\kappa_2$	$\langle \infty,\infty,1 \rangle$
$\begin{matrix} & - & \\ + & + & + \\ & + & \end{matrix}$ $\begin{bmatrix} + \\ + \\ - \end{bmatrix}$	24	$-1-\kappa_1$	$\langle \infty,2,2 \rangle$
$\begin{matrix} & - & \\ + & + & + \\ & - & \end{matrix}$ $\begin{bmatrix} + \\ + \\ - \end{bmatrix}$	24	$\kappa_1-2\kappa_2$	$\langle \infty,1,2 \rangle$
$\begin{matrix} & - & \\ + & + & - \\ & + & \end{matrix}$ $\begin{bmatrix} + \\ + \\ - \end{bmatrix}$	16	$-3\kappa_1$	$\langle 2,2,2 \rangle$
$\begin{matrix} & - & \\ + & + & - \\ & + & \end{matrix}$ $\begin{bmatrix} - \\ + \\ - \end{bmatrix}$	24	$1-\kappa_1$	$\langle 2,2,1 \rangle$
$\begin{matrix} & - & \\ + & + & + \\ & - & \end{matrix}$ $\begin{bmatrix} - \\ + \\ - \end{bmatrix}$	6	$1+3\kappa_1-2\kappa_2$	$\langle \infty,1,1 \rangle$
$\begin{matrix} & - & \\ - & + & - \\ & - & \end{matrix}$ $\begin{bmatrix} + \\ + \\ - \end{bmatrix}$	12	$2+\kappa_1+2\kappa_2$	$\langle 1,1,2 \rangle$
$\begin{matrix} & - & \\ - & + & - \\ & - & \end{matrix}$ $\begin{bmatrix} - \\ + \\ - \end{bmatrix}$	2	$3+3\kappa_1+6\kappa_2$	$\langle 1,1,1 \rangle$

are known then those for $J < 0$ can be determined by flipping every alternate spin throughout the lattice. Therefore, we shall take $J > 0$ for the rest of this paper.

The ten distinct states a cluster can take are listed in Table I. Note that their degeneracies add up to $128 = 2^7$, showing that all configurations have been included. Each cluster state can "propagate" through the lattice to give its corresponding lattice state as indicated. Hence, the

TABLE II. Stable ground states at the eight multiphase lines under discussion. μ denotes all sequences made up of bands of length two or more and $\bar{\mu}$ denotes those containing only one- and two-bands. The last two degenerate sets are explained further in Fig. 6.

	Neighboring phases		Degenerate set at boundary
1	$\langle \infty,\infty,\infty \rangle$	$\langle \infty,\infty,2 \rangle$	$\langle \infty,\infty,\mu \rangle$
2	$\langle \infty,\infty,1 \rangle$	$\langle \infty,\infty,2 \rangle$	$\langle \infty,\infty,\bar{\mu} \rangle$
3	$\langle \infty,\infty,2 \rangle$	$\langle \infty,2,2 \rangle$	$\langle \infty,\mu,2 \rangle$
4	$\langle \infty,2,2 \rangle$	$\langle 2,2,2 \rangle$	$\langle \mu,2,2 \rangle$
5	$\langle \infty,\infty,1 \rangle$	$\langle \infty,2,1 \rangle$	$\langle \infty,\mu,1 \rangle$
6	$\langle \infty,\infty,\infty \rangle$	$\langle 2,2,2 \rangle$	$\langle \mu,\mu,\mu \rangle$
7	$\langle \infty,\infty,1 \rangle$	$\langle \infty,2,2 \rangle$	$\langle \infty,n,1^{n-2}2 \rangle$ and "onions"
8	$\langle \infty,2,1 \rangle$	$\langle 2,2,2 \rangle$	$\langle 2,n,1^{n-2}2 \rangle$ and "onions"

ground-state phase diagram, Fig. 4, can be determined by finding the cluster state of minimum energy for a given κ_1 and κ_2. To describe the lattice states, we have introduced a notation following Fisher and Selke.[8] The term "l-band" is used to describe l axially consecutive spins of the same sign. The notation

$$\langle l_1 l_2 \cdots l_p, m_1 m_2 \cdots m_q, n_1 n_2 \cdots n_r \rangle$$

denotes the state where there is a repeating sequence of $p(q;r)$ bands of length

$$l_1, \ldots, l_p(m_1, \ldots, m_q;\ n_1, \ldots, n_r)$$

along the $x(y;z)$ directions, respectively. For example, $\langle \infty, \infty, 2 \rangle$ represents the phase which has ferromagnetic ordering in the xy planes but antiphase ordering, $\cdots ++--++--++\cdots$, along the z axis. The last four states listed in Table I are never minimal as one can easily see by inspection of their cluster energies (although, of course, they do appear for $J<0$).

Note that $\langle \infty, 2, 2 \rangle$ describes two distinct states, with chess-board and staircase ordering, as shown in Fig. 5. This type of ground-state degeneracy, which is present in other states with a modulation in at least two axial directions, is broken by entropy, as will be explained in the next section.

There are an infinite number of degenerate ground states along the bold phase boundaries (called multiphase lines[8]) in Fig. 4. The degenerate set of states at each multiphase line, which are constructed from the two types of cluster states which make up the neighboring phases, are listed in Table II. Note that the first five of these have structural sequences which vary in just one of the axial directions, whereas the sixth has the same varying sequence, organized in a staircaselike structure, in all three axial directions. Thus, one can consider this structure as having a sequence of bands which propagate in a $\langle 111 \rangle$ direction. This can best be seen from considering the two distinct cluster states which make up this structure.

The last two degenerate sets of states listed in Table II

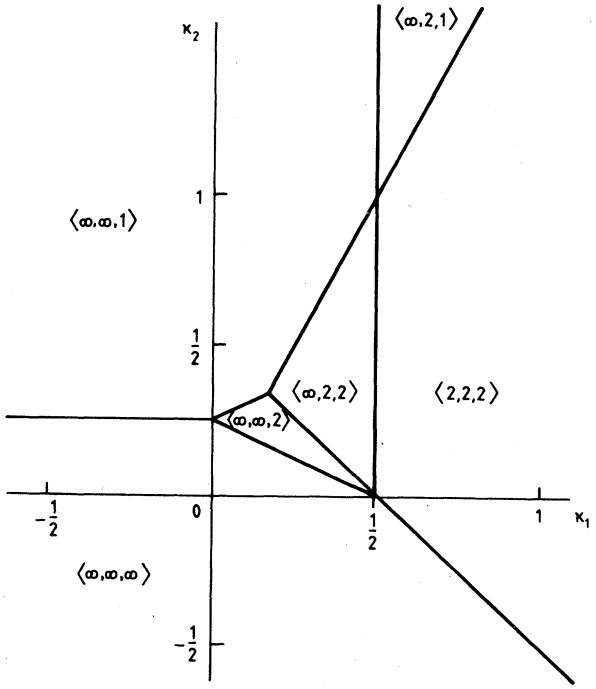

FIG. 4. Ground-state phase diagram of the Hamiltonian (2.1). The bold lines denote multiphase lines.

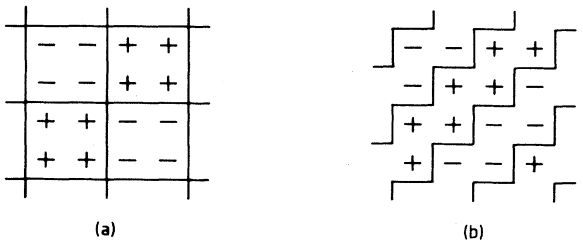

FIG. 5. The two degenerate states represented by $\langle \infty, 2, 2 \rangle$ showing (a) chessboard ordering and (b) staircase ordering, in the yz plane.

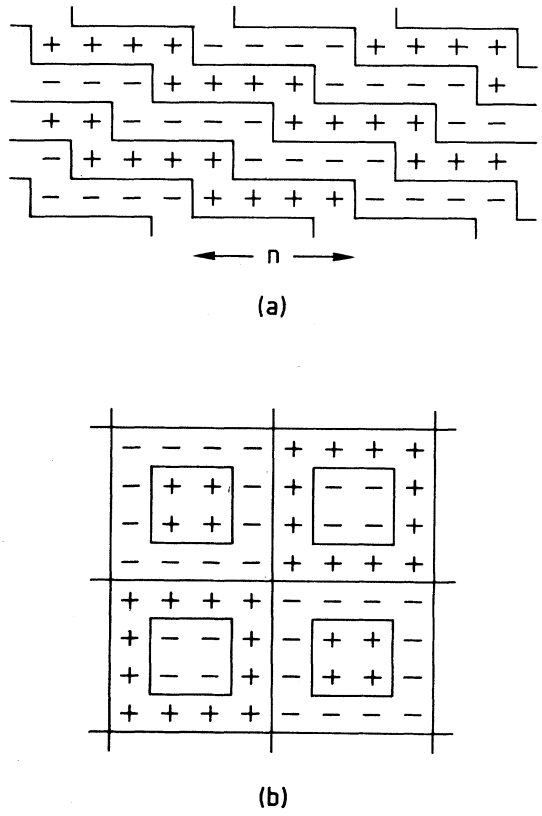

FIG. 6. Degenerate ground states appearing in the last two entries in Table II. (a) shows the ordering in the yz planes for states represented by $\langle \infty, n, 1^{n-2}2 \rangle$ and $\langle 2, n, 1^{n-2}2 \rangle$ (in this case with $n=4$) and (b) illustrates the "onionlike" ordering for "single-skinned" onions.

are somewhat more complicated. They include states represented by $\langle \infty, n, 1^{n-2}2 \rangle$ ($\langle 2, n, 1^{n-2}2 \rangle$) with $n=3,4,\ldots,$ for the seventh (eighth) degenerate set. In the *yz* planes the spins are arranged as shown in Fig. 6(a) such that only one skew staircase structure is found for each n. The other states found along these multiphase lines are those with "onionlike" ordering. Again, the ordering along the x direction is ferromagnetic [(2,2)-antiphase] for the seventh (eighth) degenerate set. In the *yz* planes, the configurations are composed from onionlike antirepeat units. Each antirepeat unit consists of four spins arranged in a square which is then surrounded by one or more onion skins, each with a thickness of one lattice spacing and succeeded by an onion skin of opposite spin. An example illustrating one-skin onions is shown in Fig. 6(b).

Of special interest to us are the ground states at the superdegenerate point $(\kappa_1,\kappa_2)=(\frac{1}{2},0)$. At this point, the ground state may contain fully frustrated spins (spins that can flip without any cost in energy). Indeed, as argued in Sec. V, the presence of these spins results in one third of the $\{111\}$ planes becoming disordered at all nonzero temperatures provided one is close enough to the superdegenerate point. In addition, the zero-temperature entropy per spin at this point becomes nonvanishing, whereas throughout the rest of the phase diagram, including even the multiphase lines, it remains zero.

III. CHESSBOARD VERSUS STAIRCASE ORDERING

It was pointed out in the last section that in the region where $\langle \infty,2,2 \rangle$ provides the ground state, the chessboard structure [Fig. 5(a)] and the staircase structure [Fig. 5(b)] are degenerate. In addition, there are translational degeneracies within the structural ones but these will not be given further consideration since they play little role in the subsequent thermodynamics. Consider also the ground states represented by $\langle 2,2,2 \rangle$. Here there is a fivefold structural degeneracy which includes a state with chessboard ordering in all of its $\{100\}$ planes, a state with staircase ordering in all the $\{100\}$ planes and three states containing both chessboard and staircase ordered planes in differing proportions. In this section we provide arguments, based on low-temperature series expansions, which show how the ground-state degeneracies of $\langle \infty,2,2 \rangle$ and $\langle 2,2,2 \rangle$ are broken at any finite temperature.

We start by briefly explaining the method employed. The standard low-temperature series expansion starts from the decomposition of the partition function[20]

$$Z_N = e^{-\beta N E_0}\left[1+\sum_{m=1}\Delta Z_N(m)\right], \tag{3.1}$$

where Z_N is the canonical partition function for a system of N spins, E_0 is the ground-state energy per spin, $\beta=1/k_BT$ and $\Delta Z_N(m)$ is the contribution to the partition function which comes from flipping m spins from their ground-state values. If F is the free energy of the system, then the reduced free energy per spin, f, is

$$f=-\frac{\beta F}{N}=-\beta E_0+{\sum_{m=1}}'\frac{\Delta Z_N(m)}{N}, \tag{3.2}$$

where the prime in the sum indicates that only contributions from $\Delta Z_N(m)$ that are linear in N are included; this being a consequence of the "linked cluster" theorem.[20] The thermodynamically stable phase is that which maximizes f.

The $\langle \infty,2,2 \rangle$ states will be considered first. The contribution to f coming from E_0 and from flipping three spins or less is the same for both chessboard and staircase phases. A little thought shows that the first excitations that differentiate the free energies come from flipping four *coupled* spins that lie in the same $\{100\}$ plane. There are hundreds of such excitations but most of them given equal contributions to the free energy of both phases and only the three displayed in Table III will contribute to the free-energy difference to leading order. Throughout the region of the ground-state phase diagram occupied by $\langle \infty,2,2 \rangle$ we have that $0<\kappa_2<1$ for which, as seen from Table III, spin-flip configurations coming from excitations about the chessboard structure dominate (that is, makes a larger contribution to its reduced free energy). Hence, chessboard ordering is favored over staircase ordering for $\langle \infty,2,2 \rangle$ at low temperatures.

We now consider the five $\langle 2,2,2 \rangle$ states. Since these states are composed of chessboard and staircase planes in differing proportions, the same configurations as before contribute to their relative reduced free energies to leading order. The corresponding Boltzmann weights are also listed in Table III. In this case we can see that excitations from chessboard planes dominate for $\kappa_2<1$ but those from staircase planes dominate when $\kappa_2>1$. Recall

TABLE III. Configurations of flipped spins that make the leading contributions to the reduced free energy differences of the chessboard and staircase phases. In the "counts" column, "c" means that the configuration occurs in chessboard planes only while "s" means it occurs only in staircase planes. x is the elementary Bolzmann weight defined by $x=\exp(-2\beta J)$.

Spin-flip configuration	Count per planar site	Boltzmann weights $\langle \infty,2,2 \rangle$	Boltzmann weights $\langle 2,2,2 \rangle$	Dominant when
+ + + +	$\frac{1}{4}c$	$x^{8\kappa_1+4\kappa_2}$	$x^{-8+24\kappa_1+4\kappa_2}$	$\kappa_2<\frac{2}{3}$
− − + +	$1c$	$x^{4+8\kappa_1-2\kappa_2}$	$x^{-4+24\kappa_1-2\kappa_2}$	$\frac{2}{3}<\kappa_2<1$
− − + +	$1s$	$x^{6+8\kappa_1-4\kappa_2}$	$x^{-2+24\kappa_1-4\kappa_2}$	$1<\kappa_2$

that the region where $\langle 2,2,2 \rangle$ is the ground state extends across all values of κ_2. Hence, from knowing which configurations dominate, all planes take chess-board ordering when $\kappa_2 < 1$ while for $\kappa_2 > 1$ all planes favor staircase ordering. This will be true for sufficiently low temperatures and mixed states will not be found at these temperatures. So there is an interesting first-order phase transition which occurs along $(\kappa_1 > \frac{1}{2}, \kappa_2 = 1)$.

Before proceeding to describe the mean-field theory for the model, it should be pointed out that a mean-field approximation of the Bragg-Williams type, as described in the next section and used throughout the rest of this paper, is not capable of determining differences in the free energies between the chessboard and staircase phases. In order to do this within mean-field theory, one would need to use a higher cluster-variation approach such as the Kikuchi method.[21]

IV. THE MEAN-FIELD THEORY

A. The mean-field equations

We now describe the results of a mean-field approximation applied to the Hamiltonian (2.1). As usual with these types of models, it is convenient to start from the Bogoliubov inequality for the free energy F,

$$F \leq \Phi \equiv F_0 + \langle \mathcal{H} - \mathcal{H}_0 \rangle_0 , \tag{4.1}$$

where $\mathcal{H}_0$ is some trial Hamiltonian, F_0 the corresponding free energy and $\langle \cdots \rangle_0$ represents the ensemble average with respect to $\mathcal{H}_0$. The mean-field equations are obtained by using

$$\mathcal{H}_0\{S\} = -\sum_{\mathbf{r} \in \mathbb{Z}^3} H_{\mathbf{r}} S_{\mathbf{r}} \tag{4.2}$$

as a trial Hamiltonian with $H_{\mathbf{r}}$ being treated as a variational parameter. The mean-field free energy per spin is then defined as

$$F_{\mathrm{mf}} = N^{-1} \min_{H_{\mathbf{r}}} \Phi , \tag{4.3}$$

from which one obtains the following mean-field equations:

$$F_{\mathrm{mf}}\{m_{\mathbf{r}}\} = N^{-1} \sum_{\mathbf{r} \in \mathbb{Z}^3} [-k_B T \ln(2 \cosh \beta H_{\mathbf{r}}) + \tfrac{1}{2} H_{\mathbf{r}} m_{\mathbf{r}}] , \tag{4.4a}$$

$$m_{\mathbf{r}} = \tanh \beta H_{\mathbf{r}} , \tag{4.4b}$$

$$H_{\mathbf{r}} = \sum_{\mathbf{r}' \in \mathbb{Z}^3} \mathcal{J}(\mathbf{r} - \mathbf{r}') m_{\mathbf{r}'} , \tag{4.4c}$$

where $m_{\mathbf{r}} = \langle S_{\mathbf{r}} \rangle_0$ is the magnetization at site $\mathbf{r}$.

In order to evaluate F_{mf}, one needs to find solutions to Eqs. (4.4b) and (4.4c) which consist of N coupled transcendental equations. In the thermodynamic limit, these support an infinite number of solutions. It is, therefore, extremely difficult to obtain the complete mean-field phase diagram for all temperatures. However, the equations are useful in determining the phase diagram for temperatures close to the order-disorder transition temperature, $T_c(\kappa_1, \kappa_2)$, and for low temperatures. We treat each of these cases in turn.

B. Phase diagram at T_c

Close to T_c, $m_{\mathbf{r}}$ is small so that, following Elliott,[7] (4.4b) can be linearized to obtain

$$m_{\mathbf{r}} \approx \beta H_{\mathbf{r}} . \tag{4.5}$$

One then introduces the Fourier transform

$$m_{\mathbf{r}} = \sum_{\mathbf{q}} \exp(i \mathbf{r} \cdot \mathbf{q}) m_{\mathbf{q}}, \quad \mathbf{q} = (q_x, q_y, q_z) , \tag{4.6}$$

using which (4.5) becomes

$$m_{\mathbf{q}} \approx \beta J(\mathbf{q}) m_{\mathbf{q}} , \tag{4.7}$$

where

$$\frac{J(\mathbf{q})}{2J} = \cos q_x + \cos q_y + \cos q_z - \kappa_1(\cos 2q_x + \cos 2q_y + \cos 2q_z) - 2\kappa_2(\cos q_x \cos q_y + \cos q_y \cos q_z + \cos q_z \cos q_x) . \tag{4.8}$$

When $k_B T > \max_{\{\mathbf{q}\}} J(\mathbf{q})$ only a trivial ($m_{\mathbf{q}} = 0$) solution to (4.7) exists. Therefore the Curie temperature satisfies

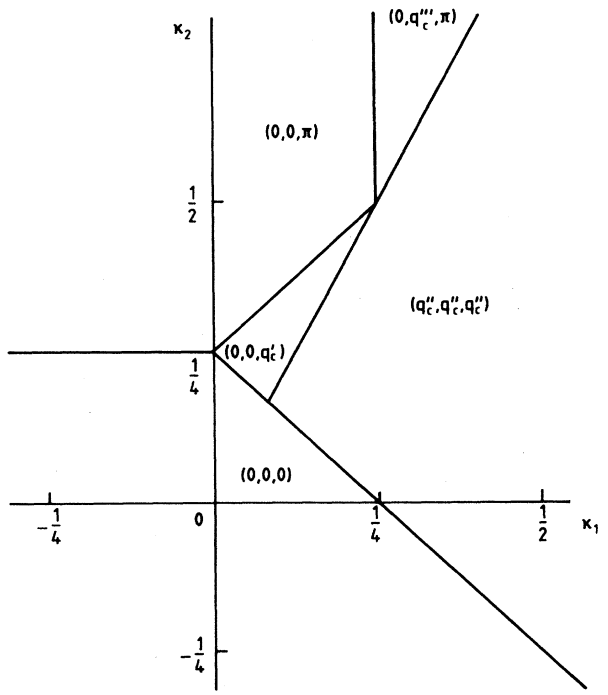

FIG. 7. Mean-field phase diagram at the order-disorder transition temperature. The critical wave vector is given for each phase with $0 \leq q_c' \leq \pi$, $0 \leq q_c'' \leq \pi/2$, and $0 \leq q_c''' \leq \pi/2$.

TABLE IV. The critical wavevectors, $\mathbf{q}_c$, and the corresponding Curie temperatures, T_c, for the phases displayed in Fig. 7.

$\mathbf{q}_c$	$k_B T_c/J$
Ferro., (0,0,0)	$6(1-\kappa_1-2\kappa_2)$
$(0,0,\pi)$	$2(1-3\kappa_1+2\kappa_2)$
$(0,0,q_c')$, $\cos q_c'=\frac{1-4\kappa_2}{4\kappa_1}$	$4-2\kappa_1-4\kappa_2+\frac{(1-4\kappa_2)^2}{4\kappa_1}$
(q_c'',q_c'',q_c''), $\cos q_c''=\frac{1}{4(\kappa_1+\kappa_2)}$	$\frac{3}{4(\kappa_1+\kappa_2)}+6\kappa_1$
$(0,q_c''',\pi)$, $\cos q_c'''=\frac{1}{4\kappa_1}$	$\frac{1}{4\kappa_1}-2\kappa_1+4\kappa_2$

$$k_B T_c(\kappa_1,\kappa_2)=\max_{\{\mathbf{q}\}} J(\mathbf{q})=J(\mathbf{q}_c)\ , \tag{4.9}$$

from which one obtains $\mathbf{q}_c(\kappa_1,\kappa_2)$, the wave vector describing the ordering at T_c. This is displayed in Fig. 7, which shows the phase diagram at the Curie temperature, T_c.

Notice that there are three regions with incommensurate order; two with modulation in just one axial direction and one with modulation in all three. The critical wave vectors and Curie temperatures for the various regions in Fig. 7 are displayed in Table IV. Note that, in contrast to the situation at zero temperature, incommensurate equivalents to phases such as $\langle \infty,2,2\rangle$, $\langle \infty,2,\mu\rangle$, and $\langle 2,2,\mu\rangle$ are absent at T_c except along $\kappa_2=2\kappa_1$ where one can find critical wave vectors obeying

$$\mathbf{q}_c=(q_{cx},q_{cy},q_{cz}),\quad \cos q_{cx}+\cos q_{cy}+\cos q_{cz}=\frac{1}{4\kappa_1}\ . \tag{4.10}$$

A more detailed description of the phase diagram confined to this line only has been given by Dawson[12] and Dawson *et al.*[13] Observe that all the phase boundaries on the right-hand plane ($\kappa_1>0$) of Fig. 6, except the one along $\kappa_2=2\kappa_1$, are Lifshitz-type;[22]; that is to say that $\mathbf{q}_c$ and the gradients of the order-disorder transition surface [in (T,κ_1,κ_2)-space] change continuously across the phase boundaries, whereas across $\kappa_2=2\kappa_1$ there are discontinuities in these quantities.

Further insight into the order-disorder transition surface can be obtained by applying the Fourier transform (4.6) to the Taylor expansion of (4.4a). This leads to the following Ginzburg-Landau expression for the free energy:

$$F_{\rm mf}\{m_{\mathbf{q}}\}=-k_B T\ln 2+\frac{1}{2}\sum_{\mathbf{q}_1,\mathbf{q}_2}[k_B T-J(\mathbf{q}_1)]m_{\mathbf{q}_1}m_{\mathbf{q}_2}\Delta(\mathbf{q}_1+\mathbf{q}_2)$$
$$+\frac{1}{2}\sum_{n=2}^{\infty}\frac{k_B T}{n(2n-1)}\sum_{\mathbf{q}_1,\ldots,\mathbf{q}_{2n}} m_{\mathbf{q}_1}\cdots m_{\mathbf{q}_{2n}}\Delta(\mathbf{q}_1+\mathbf{q}_2+\cdots+\mathbf{q}_{2n})\ , \tag{4.11a}$$

$$\Delta(\mathbf{q}_1+\mathbf{q}_2+\cdots+\mathbf{q}_{2n})=\delta^{(3)}(\mathbf{q}_1+\mathbf{q}_2+\cdots+\mathbf{q}_{2n}+2\pi\mathbf{l}),\quad \mathbf{l}\in\mathbb{Z}^3\ . \tag{4.11b}$$

The condition for a second-order phase transition between $m_{\mathbf{q}}=0,\forall\mathbf{q}$ to $m_{\mathbf{q}_c}\neq 0$ is that

$$\min_{\{\mathbf{q}\}}[k_B T-J(\mathbf{q})]=0\ ,$$

which is equivalent to (4.9). Hence, the order of the phase transition is established. By including umklapp ($\mathbf{l}\neq 0$) terms in (4.11), it should prove possible to show that commensurate phases lock-in for temperatures just below T_c.

We end the discussion in this section by pointing out that some of the important qualitative properties of the phase diagram near T_c, in particular the transition from incommensurate order in one to all three axial directions (or equivalently from a $\langle 001\rangle$ to a $\langle 111\rangle$ direction), are also found in a more general phenomenological model described within Landau theory. This is expounded in the Appendix.

C. Phase diagram at low temperatures

For temperatures close to zero, there are standard numerical techniques for treating Eqs. (4.4).[9,17] These involve direct iteration of Eqs. (4.4b) and (4.4c) for various initial trial configurations of $\{m_{\mathbf{r}}\}$. The mean-field free energies of the self-consistent solutions are then compared using (4.4a). Periodic trial configurations were used with periods equal to those of the low wavelength ground states, since by analogy with the ANNNI model, such phases are believed to dominate the low-

temperature phase diagram. These are, of course, only a subset of the infinite number of possible solutions given by (4.4b) and (4.4c). In general, the wavelength is preseved by the iterations.

The low-temperature mean-field phase diagrams, all at constant κ_2, in the vicinity of the first six multiphase lines listed in Table II, are shown in Fig. 8. These were obtained using the method described above with a numerical accuracy of, typically, seven decimal figures. Through an increase in precision one observes more commensurate phases with higher periodicities. For the last two multiphase lines listed in Table II, we were unable to detect for any low temperature, at least for the numerical precision employed, any stable intervening phases

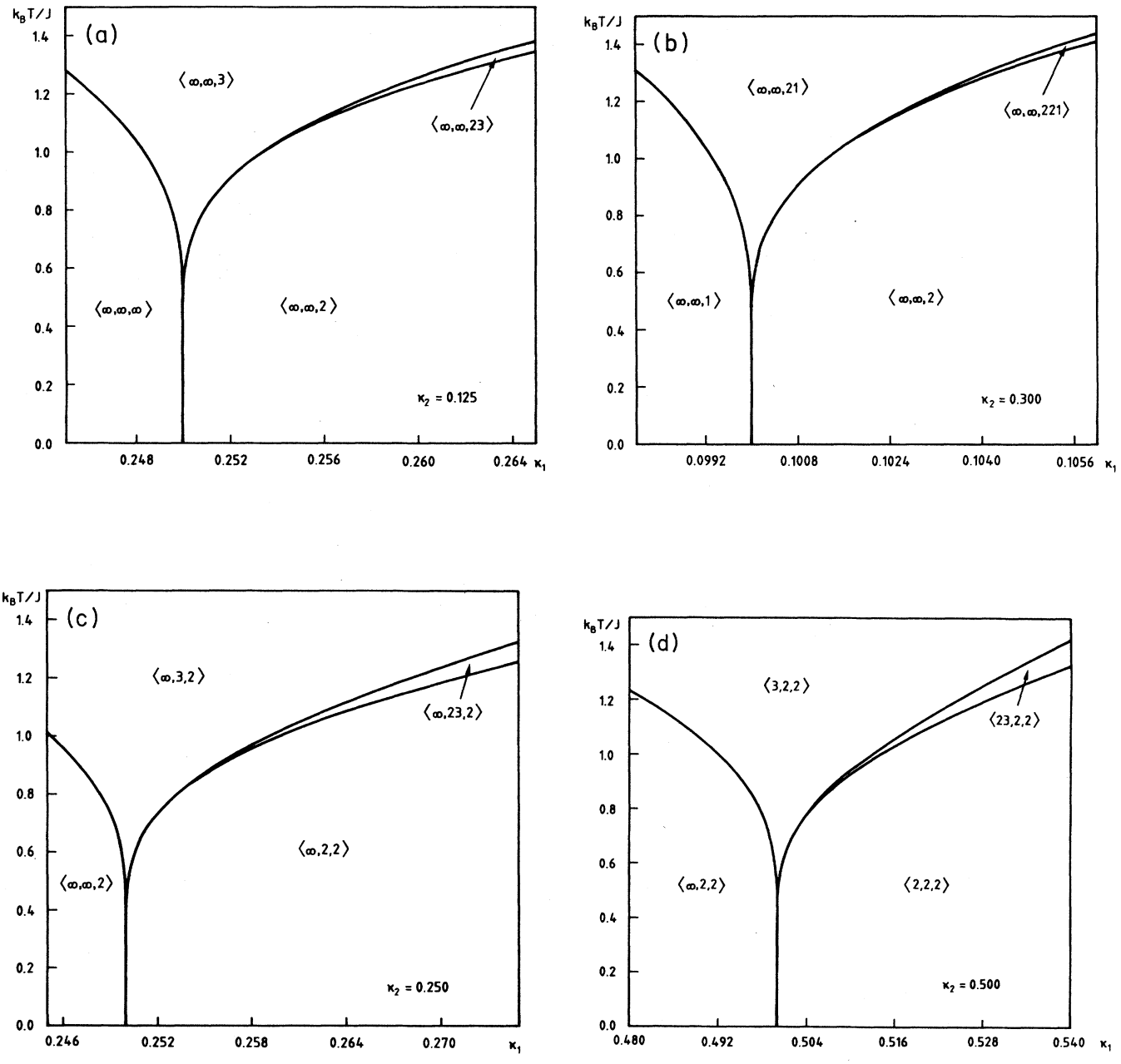

FIG. 8. Low-temperature mean-field phase diagram in the vicinity of the first six multiphase lines listed in Table II. Other commensurate phases are found if the numerical precision is increased. (a) the $\langle \infty, \infty, \mu \rangle$ phases (b) the $\langle \infty, \infty, \bar{\mu} \rangle$ phases (c) the $\langle \infty, \mu, 2 \rangle$ phases (d) the $\langle \mu, 2, 2 \rangle$ phases (e) the $\langle \infty, \mu, 1 \rangle$ phases (f) the $\langle \mu, \mu, \mu \rangle$ phases.

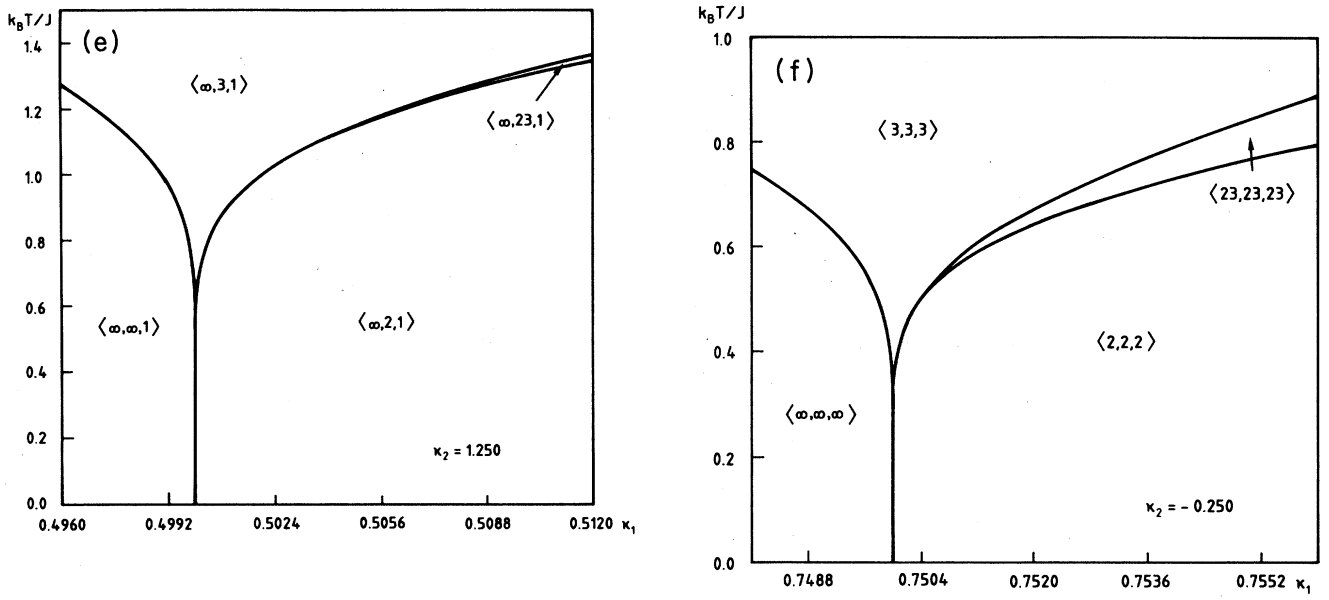

FIG. 8. (*Continued*).

separating the two neighboring phases of the multiphases lines. Therefore, it seems plausible that single first-order phase boundaries separating $\langle \infty,\infty,1 \rangle$ from $\langle \infty,2,2 \rangle$ and $\langle \infty,1,2 \rangle$ from $\langle 2,2,2 \rangle$ persist at (low) finite temperatures without any intervening phases.

The similarity between the shape of the phase boundaries and the form of the phase sequences, displayed in Fig. 8, and those of the ANNNI model is striking but not surprising. This is because each of the top six degenerate sets in Table II has a modulation which varies in one direction only which is either axial (for the first five cases) or along $\langle 111 \rangle$ (for the $\langle \mu,\mu,\mu \rangle$ phases). It is therefore possible, within the mean-field approximation at low temperatures, to map each of these phase sequences onto those of the ANNNI model via a reidentification of the ANNNI model coupling constants.[11] Before explaining this further, it will be helpful to give a brief review of the ANNNI model.[1-3,7-9]

The Hamiltonian of the ANNNI model is

$$\mathcal{H}\{S\} = -J_0 \sum_{\mathrm{NN}}{}^{\perp} S_{\mathbf{r}} S_{\mathbf{r}'} - J_1 \sum_{\mathrm{NN}}{}^{z} S_{\mathbf{r}} S_{\mathbf{r}'} - J_2 \sum_{\mathrm{NNN}}{}^{z} S_{\mathbf{r}} S_{\mathbf{r}'} , \tag{4.12}$$

where the spins $S_{\mathbf{r}} = \pm 1$ occupy sites of a cubic lattice. The first sum is over nearest neighbor (NN) pairs within xy-planes and the remaining sums are over nearest neighbor and next-nearest neighbor (NNN) pairs along the z direction. The mean-field phase diagram for this model (after Duxbury and Selke[17]) is shown in Fig. 9, for the case where $J_1 > 0$. Note how a "Devil's flower" of phases springs from the multiphase point $-J_2/|J_1| = 1/2$. The Fisher-Selke notation[8] is used to label the phases and is explained as follows. Ordering in the xy planes is always ferromagnetic ($J_0 > 0$) and $\langle n_1 n_2, \ldots, n_p \rangle$ denotes a repeating sequence of p bands (which in this case are consecutive xy layers with the same spin) of length $n_1, n_2, \ldots, n_p$. The Hamiltonian is invariant under $J_1 \to -J_1$ provided $S_{\mathbf{r}} \to -S_{\mathbf{r}}$ for every alternate xy plane. Hence, the phase boundaries for $J_1 < 0$ will be identical to those of Fig. 9 but the phases will now be made up of only one- and two-bands.

Returning to the model, (2.1), it is easy to see that for trial configurations corresponding to the first six degenerate sets listed in Table II, the mean-field equations, (4.4), remain identical to those of the ANNNI model with coupling constants J_0, J_1, and J_2 taking appropriate values as indicated in Table V. This then explains the similarities between the phase diagrams of Fig. 8 and that of Fig. 9.

A mapping similar to the first one listed in Table V was used by Widom *et al.*[11] although it was first attributed to M. E. Fisher. Of course, in our case, unlike the ANNNI model, the ordering within the planes perpendicular to the direction of modulation will not always be ferromagnetic but may be either ferromagnetic, (2,2)-antiphase, or a mixture depending on the phase sequence under consideration. This can easily be accounted for by making the appropriate changes to J_0 and J_1.

Note that for the mappings listed in Table V, the six multiphase lines correspond to having $-J_2/|J_1| = 1/2$ in each case, as expected. Also observe that for the first mapping, $J_1 > 0$ when $\kappa_2 < 1/4$ but $J_1 < 0$ when $\kappa_2 > 1/4$. This is consistent with the fact that Fig. 8(a) ($\kappa_2 < 1/4$) contains only phases with bands of length two or more while Fig. 8(b) ($\kappa_2 > 1/4$) contains only phases made up of one- and two-bands.

One should stress that Figs. 8(a), 8(b), 8(d), and 8(e) differ from the mean-field phase diagram of the ANNNI model in that in these cases J_0 is not independent of $-J_2/|J_1|$. The phase boundaries are therefore distorted, as opposed to just rescaled, versions of those in Fig. 9. It is also important to select the correct temperature range

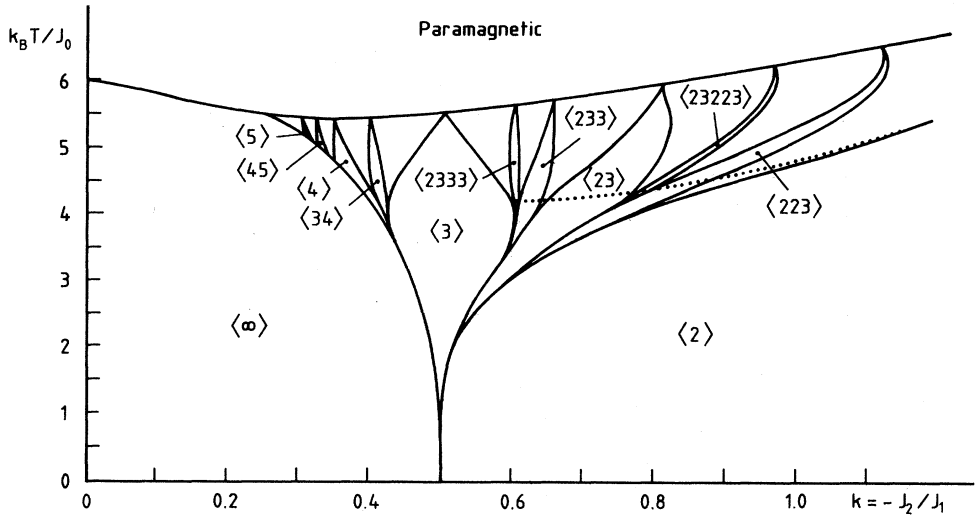

FIG. 9. Mean-field phase diagram of the ANNNI model showing the main commensurate phases (after Selke and Duxbury[17]). The dotted line estimates the boundary above which incommensurate phases are found.[9]

for the mean-field mappings to the ANNNI model to be applicable since in some regions of the phase diagram, as the temperature is increased, the modulated phases springing from different multiphase lines will interfere with one another.

At this stage, it is useful to make comparisons with the phase diagram at T_c. Firstly, the Devil's flowers springing from the two multiphase lines containing the phase sequences $\langle \infty,\infty,2^j3 \rangle$ and $\langle \infty,\infty,2^j1 \rangle$ both appear to join with the triangle in Fig. 7 containing the phase with critical wave vector $(0,0,q_c')$. The first of these phase sequences is found in that part of the triangle with $\kappa_2 < 1/4$ while the second is found for $\kappa_2 > 1/4$. $\langle \infty,\infty,2 \rangle$ is found at T_c along $\kappa_2 = 1/4$. Clearly, the phases with critical wave vectors (q_c'',q_c'',q_c'') and $(0,\pi,q_c''')$ are linked to the phase sequences $\langle \mu,\mu,\mu \rangle$ and $\langle \infty,1,\mu \rangle$, respectively. As for the phase sequences $\langle \infty,2,\mu \rangle$ and $\langle 2,2,\mu \rangle$, these seem to disappear with increasing temperature except along $\kappa_2 = 2\kappa_1$.

Another interesting observation concerns the mappings in Table V and the phase diagram at T_c. For the ANNNI model, the critical wave vector q_c is given, in the modulated region, as $\cos q_c = 1/(4\kappa)$ where $\kappa = -J_2/|J_1|$. In our model the critical wave vectors for the modulated phases corresponding to $\langle \infty,\infty,\mu \rangle$, $\langle \infty,1,\mu \rangle$, and $\langle \mu,\mu,\mu \rangle$ are related to $-J_2/|J_1|$, as given by their mean-field mappings of Table V, in exactly the same way as can easily be seen from Table IV.

Let us now consider more closely the multiphase line $(\kappa_1+\kappa_2 = 1/2)$ containing only the phases labeled $\langle \mu,\mu,\mu \rangle$. As mentioned before, these can be regarded as structures having ferromagnetic ordering within a set of parallel $\{111\}$ planes with the commensurate order manifesting itself as a repeating sequence of bands which propagate in a $\langle 111 \rangle$ direction. An example of such a structure, $\langle 3,3,3 \rangle$, is shown in Fig. 10. The mean-field phase diagram near this multiphase line, Fig. 8(f), has the property that as one gets closer to the superdegenerate point $(\kappa_1 = 1/2, \kappa_2 = 0)$ the region occupied by the

TABLE V. Values taken by the coupling constants of the ANNNI model which leave the mean-field equations, (4.4), identical to those of the ANNNI model whose states are represented by $\langle \mu \rangle$. For the first entry, μ can be *either* any state with bands of length two or more ($\kappa_2 < 1/4$) or those with one- and two-bands only ($\kappa_2 > 1/4$). For the other four, μ denotes only those states with bands of length two or more.

Type of phase	Mapping to the coupling constants of the ANNNI model
$\langle \infty,\infty,\mu \rangle$	$J_0 = (1-\kappa_1-\kappa_2)J$ $J_1 = (1-4\kappa_2)J$ $J_2 = -\kappa_1 J$
$\langle \infty,2,\mu \rangle$	$J_0 = \frac{1}{2}J$ $J_1 = (1-2\kappa_2)J$ $J_2 = -\kappa_1 J$
$\langle 2,2,\mu \rangle$	$J_0 = \kappa_1 J$ $J_1 = J$ $J_2 = -\kappa_1 J$
$\langle \infty,1,\mu \rangle$	$J_0 = (\kappa_2-\kappa_1)J$ $J_1 = J$ $J_2 = -\kappa_1 J$
$\langle \mu,\mu,\mu \rangle$	$J_0 = -\frac{3}{2}\kappa_2 J$ $J_1 = 3J$ $J_2 = -3(\kappa_1+\kappa_2)J$

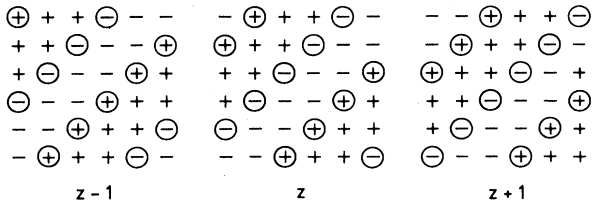

FIG. 10. One of the ground states, $\langle 3,3,3\rangle$, degenerate along the multiphase line with $\kappa_2<0$. Planes are shown for successive values of z. When $\kappa_2=0$, the encircled spins become fully frustrated.

"Devil's flower" rapidly broadens. That this happens can readily be seen from the mappings in Table V, where approaching the superdegenerate point corresponds to having $J_0\to 0$ in the equivalent ANNNI model. This phenomenon is also consistent with the rapid increase, as $\kappa_2\to 0$, in the contributions to the entropy coming from spins which lie on the edge of bands of length three or more. These include the encircled spins of Fig. 10. When $\kappa_2=0$ these spins become fully frustrated which has a dramatic effect on the phase diagram as will be explained in the next section.

One should recall the failure of this (Bragg-Williams) type of mean-field theory to detect differences in the free energy between the chessboard and staircase ordering for $\langle \infty,2,2\rangle$ and $\langle 2,2,2\rangle$. The preference of the chessboard ordered $\langle 2,2,2\rangle$ phase when $\kappa_2<1$, found in Sec. III, would affect the phase diagram near the multiphase line $\kappa_1+\kappa_2=1/2$, as follows. Mean-field theory predicts that the phase sequence $\langle 2^j3,2^j3,2^j3\rangle$, with arbitrarily large j, would spring from this line. However, these phases can be considered as a sequence of equally spaced three bands (occupying $\{111\}$ planes) amid a matrix of $\langle 2,2,2\rangle$ ordering which is forced to be staircaselike. This we know to be unfavorable and hence we would expect a maximum j above which $\langle 2^j3,2^j3,2^j3\rangle$ would become unstable compared to chessboard ordered $\langle 2,2,2\rangle$.

V. THE SUPERDEGENERATE POINT

When $(\kappa_1,\kappa_2)=(1/2,0)$ it is possible to construct ground states containing fully frustrated spins which are spins that can flip without changing the energy. These states have a nonzero entropy per spin at zero temperature, with each fully frustrated spin making a contribution of at least $k_B\ln 2$ to the zero-point entropy. Hence, we have termed $(\kappa_1,\kappa_2,T)=(1/2,0,0)$ the superdegenerate point. Clearly, the ground state with the highest density of fully frustrated spins will give rise to the stable low-temperature phase in the vicinity of the superdegenerate point, since such a state will maximize the entropy. The ground state which does this is the state $\langle 3,3,3\rangle$ shown in Fig. 10. The encircled spins are the fully frustrated ones, with each one free to flip *independently* of any of the others. The situation described so far has similar features to the triangular antiferromagnetic Ising net studied by Wannier.[23]

The mean-field phase diagram near the superdegenerate point with $\kappa_2=0$, Fig. 11, was determined numerically as before. The mean-field approximation predicts the appearence of the $\langle 3,3,3\rangle$ phase shown in Fig. 10, with zero magnetization at each fully frustrated (encircled) site. The $\{111\}$ planes of zero magnetization can be understood as resulting from thermal fluctuations which cause these spins to flip independently without any cost in energy.

Since the entropy of the fully frustrated spins plays such a dominant role at low temperatures, one can express the free energy per spin, F, of this $\langle 3,3,3\rangle$ phase to a very good approximation for low temperatures as

$$F=E_0-\tfrac{1}{3}k_BT\ln 2,\quad E_0=-(1+\kappa_1)J\ , \tag{5.1}$$

where E_0 is the ground-state energy per spin when $\kappa_2=0$. This formula is in excellent agreement with numerical mean-field values for F. By comparing (5.1) with the ground-state energies, with $\kappa_2=0$, for $\langle \infty,\infty,\infty\rangle$ and $\langle 2,2,2\rangle$, one can obtain expressions for the phase boundaries separating $\langle \infty,\infty,\infty\rangle$ from $\langle 3,3,3\rangle$ and $\langle 3,3,3\rangle$ from $\langle 2,2,2\rangle$, which are, respectively,

$$\left[\frac{k_BT}{J}\right]_{\infty|3}\simeq\frac{6(1-2\kappa_1)}{\ln 2}\ , \tag{5.2a}$$

$$\left[\frac{k_BT}{J}\right]_{3|2}\simeq\frac{3(2\kappa_1-1)}{\ln 2}\ . \tag{5.2b}$$

These are in very good agreement with Fig. 11 and explain the apparent linear form of the phase boundaries.

The simple entropy arguments given above imply that when approaching the superdegenerate point, with $\kappa_2=0$, the $\langle 3,3,3\rangle$ phase will be the only stable phase separating $\langle \infty,\infty,\infty\rangle$ from $\langle 2,2,2\rangle$, as opposed to the usual sequence of commensurate phases of increasing wavelength. This is because as soon as the periodicity of the phase is increased from that of $\langle 3,3,3\rangle$ (or a domain wall is put in), the density of the fully frustrated spins will decrease, thus significantly reducing the entropy.

It should be stressed that the *exact* zero-point entropy

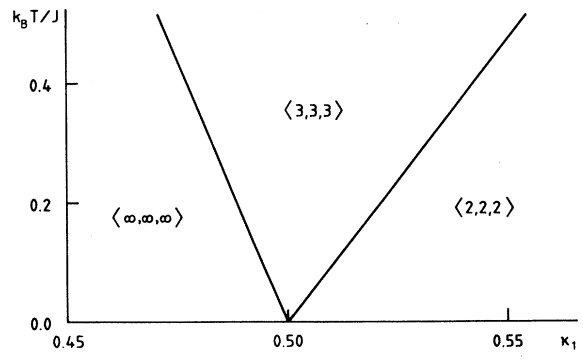

FIG. 11. Mean-field phase diagram in the vicinity of the superdegenerate point for $\kappa_2=0$. The phase denoted by $\langle 3,3,3\rangle$ is shown in Fig. 10 but, for $\kappa_2=0$, the magnetization is zero at the encircled sites.

for $\langle 3,3,3 \rangle$ will not be $(1/3)k_B \ln 2$, as given by mean-field theory, but *greater,* due to "contingent freedoms" which are also present in Wannier's problem.[23] These are contributions to the entropy due to spins which are not encircled in Fig. 10 but can still become fully frustrated when the encircled spins take certain configurations. However, the Bragg-Williams type of mean-field theory used here is incapable of taking such effects into account since it ignores correlations of large enough clusters. In fact, one cannot rule out the possibility that contingent freedoms could lead to the total destruction of the remaining order, as happens in Wannier's case,[23] leaving a disordered phase in the vicinity of the superdegenerate point.

VI. DISCUSSION

In this paper we have presented and analyzed an Ising model with competing interactions isotropic with respect to the cubic axes. The model was introduced with a view to applying it to binary alloys exhibiting long-period structural modulation. It was also found to have several interesting features in its own right.

We have studied the mean-field theory of the model both at low temperatures and near the order-disorder transition. Within this approximation the model supports all phases found in the ANNNI model[7–9] (phases modulated in just one lattice direction) together with phases, modulated in two or more lattice directions, not found in the ANNNI phase diagram yet still occurring as structural phases in some binary alloys.[5,10]

Some features of the mean-field phase diagram remain puzzling. Although the phases $\langle \infty,2,2 \rangle$, $\langle \infty,\mu,2 \rangle$, and $\langle \mu,2,2 \rangle$ occupy large regions of the low-temperature phase diagram, they seem to vanish as the temperature is raised and do not appear at all at $T_c(\kappa_1,\kappa_2)$ except along $\kappa_2=2\kappa_1$. It would be interesting to know what happens to these phases at higher subcritical temperatures.

This could be partly resolved by including Umklapp terms in the Landau theory for the model [Eq. (4.11)]. This would show which commensurate phases lock-in at temperatures just below T_c. This calculation would be particularly interesting in the vicinity of the line $\kappa_2=2\kappa_1$ because at T_c there is a degeneracy of many modulated phases (with modulation in one, two, and three lattice directions). It would also provide a link between our work and that of Dawson[12] and Dawson *et al.*[13]

One also needs to resolve the question of ordering in the vicinity of the superdegenerate point. Mean-field theory suggests that one in every three $\{111\}$ planes becomes disordered for temperatures right down to zero. However, it is possible that the whole lattice may be disordered and mean-field theory would be incapable of dealing with this. One needs to go beyond mean-field theory to determine whether long-range order is present near the superdegenerate point.

One would expect the region of parameter space which is most likely to model binary alloys to be that for which $\kappa_1<\kappa_2<1/2$. In this region, layered modulated phases dominate and, where other phases are found, chess-board ordering is preferred over staircase ordering. This appears to be in accordance with experimental observations.[5]

As regards to the chessboard and staircase phases, we have shown that both types of ordering can exist as stable phases at finite temperature with chessboard ordering being more favorable when $\kappa_2<1$ while staircase is preferred when $\kappa_2>1$. A novel phase transition, worth further investigation, separates these two types of order.

Coming back to the motivation behind the model, we reiterate that we expect the interactions between the structural units in binary alloys to be isotropic (in the absence of strain) and hence that the model we propose provides a more suitable representation of binary alloys than the ANNNI model. However, it must be stressed that we can only qualitatively predict the features of a given phase diagram. For example, note that the distance across cubic diagonals is shorter than the distance between next-nearest-neighbor sites along the cubic axes. Therefore, in a real binary alloy, the interactions extending across body diagonals could have a significant effect on the phase diagram. It would be interesting, if complicated, to see how the phase diagram is modified if these interactions were incorporated into the Hamiltonian (2.1).

Finally, it is to be hoped that band-theory calculations might lead to predictions for interaction parameters in a Hamiltonian of the form (2.1) which could lead to qualitative predictions for the behavior of specific binary alloys.

ACKNOWLEDGMENTS

We would like to thank D. B. Abraham, M. C. B. Barbosa, M. E. Fisher, D. Price, H. Röder, and W. Selke for helpful discussions and P. Jenson for kindly sending us results of his calculations before publication. One of us (P.U.) acknowledges support from the Science and Engineering Research Council (United Kingdom) through Oxford University where most of the work described here was performed and through the Condensed Matter Theory Program of the National Science Foundation (under Grant No. DMR 87-96299).

APPENDIX

Some of the qualitative aspects of the phase diagram near T_c are also found in continuum theories described by the following Ginzburg-Landau free energy functional of a single component order parameter $M(\mathbf{r})$:

$$\mathcal{F}[M]=\mathcal{F}_0+\int d^3\mathbf{r}\left[\frac{1}{2}A_0M^2+\frac{1}{4}BM^4+\frac{1}{2}\alpha\sum_{i=x,y,z}(\partial_iM)^2+\frac{1}{4}\sum_{i,j=x,y,z}(\partial_i^2M)\beta_{ij}(\partial_j^2M)\right], \tag{A1}$$

where $\partial_x=\partial/\partial x$, etc., $B>0$ and

TABLE VI. Position of the order-disorder phase transition and critical wave vector at the transition for the Landau theory defined by the free energy (A1).

$\alpha \geq 0$		Phase transition at $A_0=0$	Critical wave vector $\mathbf{q}_c$ (0,0,0)
	$\beta_1 \leq \beta_2$	$A_0=\frac{\alpha^2}{2\beta_1}$	$(0,0,(-\alpha/\beta_1)^{1/2})$
$\alpha \leq 0$	$\beta_1=\beta_2$	$A_0=\frac{\alpha^2}{2\beta_1}$	all $\mathbf{q}_c$ with $\lvert\mathbf{q}_c\rvert^2=-\alpha/\beta_1$
	$\beta_1 \geq \beta_2$	$A_0=\frac{3\alpha^2}{2(\beta_1+2\beta_2)}$	$\left[\left[\frac{-\alpha}{\beta_1+2\beta_2}\right]^{1/2},\left[\frac{-\alpha}{\beta_1+2\beta_2}\right]^{1/2},\left[\frac{-\alpha}{\beta_1+2\beta_2}\right]^{1/2}\right]$

$$\beta_{ij}=\begin{cases}\beta_1>0, & \text{for } i=j\\ \beta_2>0, & \text{for } i\neq j\end{cases}. \tag{A2}$$

This is merely a slight generalization of the Landau theories employed by previous authors to study Lifshitz points.[22] If α is positive then the usual second-order phase transition from a paramagnetic to a ferromagnetic state occurs when A_0 changes its sign from positive to negative. However, when α becomes negative one expects the ferromagnetic state to become unstable in favor of some modulated, inhomogeneous phase. Keeping both β_1 and β_2 positive prevents such a phase from having an infinitely rapid variation in its order parameter. The resulting phase diagram can be studied by following the methods of Michelson.[22]

(A1) is Fourier transformed, using the transform displayed in (4.6), to obtain

$$\mathcal{F}\{M_{\mathbf{q}}\}-\mathcal{F}_0=\frac{1}{2}\sum_{\mathbf{q}}A_{\mathbf{q}}|M_{\mathbf{q}}|^2+\frac{1}{4}B\sum_{\mathbf{q}+\mathbf{q}'+\mathbf{q}''+\mathbf{q}'''=0}M_{\mathbf{q}}M_{\mathbf{q}'}M_{\mathbf{q}''}M_{\mathbf{q}'''}\ , \tag{A3}$$

where

$$A_{\mathbf{q}}=A_0+\alpha\sum_{i=x,y,z}q_i^2+\frac{1}{2}\sum_{i,j=x,y,z}q_i^2\beta_{ij}q_j^2\ . \tag{A4}$$

Lattice effects in the form of Umklapp terms have been ignored. The second-order phase transition from the disordered ($M_{\mathbf{q}}=0,\forall\mathbf{q}$) to the ordered ($M_{\mathbf{q}_c}\neq 0$) state occurs when $\min_{\{\mathbf{q}\}}A_{\mathbf{q}}=A_{\mathbf{q}_c}$ changes sign. The critical wave vector $\mathbf{q}_c$ which describes the ordering at the order-disorder surface depends on α, β_1, and β_2 as Table VI.

The usual Lifshitz point[22] is found at $\alpha=0$, that is for $\alpha>0$ ferromagnetic ordering is found while for $\alpha<0$ modulated order is stable. However in the $\alpha<0$ region one finds modulation in just one axial direction (in other words modulation along a $\langle 100\rangle$ direction) when $\beta_1\leq\beta_2$ (that is where the off-diagonal elements of β_{ij} dominate) and modulation in all three axial directions (modulation along a $\langle 111\rangle$ direction) when $\beta_1\geq\beta_2$ (diagonal elements of β_{ij} dominate). So an interesting phase transition from modulated order in a $\langle 100\rangle$ direction to modulated order in a $\langle 111\rangle$ direction can be obtained within the context of a Landau theory of the form expressed in (A1).

Finally, if one expands $J(\mathbf{q}_1)$, in (4.11a), for small $\mathbf{q}_1$, while ignoring the Umklapp terms, one can obtain (A3) and (A4) from the following identifications:

$$\begin{aligned}A_0&=k_BT-2J(3-3\kappa_1-6\kappa_2)\ ,\\ \alpha&=J(1-4\kappa_1-4\kappa_2)\ ,\\ \beta_1&=\tfrac{1}{6}J(16\kappa_1+4\kappa_2-1)\ ,\\ \beta_2&=\kappa_2J\ ,\\ B&=\tfrac{1}{3}k_BT\ ,\end{aligned} \tag{A5}$$

showing the equivalence of the original microscopic model, (2.1), to the Landau theory (A1) provided that $\mathbf{q}$ is small, so that one is close to the Lifshitz "line."

[1] P. Bak, Rep. Prog. Phys. **45**, 587 (1982).
[2] J. Yeomans, Solid State Phys. **41**, 151 (1988).
[3] W. Selke, Phys. Rep. **170**, 213 (1988).
[4] A. Loiseau, G. van Tendeloo, R. Portier, and F. Ducastelle, J. Phys. (Paris) **46**, 595 (1985).
[5] D. Broddin, G. van Tendeloo, J. van Landuyt, S. Amelinckx, R. Portier, M. Guymont, and A. Loiseau, Philos. Mag. **A54**, 385 (1987).
[6] J. Kulik and D. de Fontaine, in *Phase Transformations in Solids*, edited by T. Tsakalakos (North-Holland, New York, 1984), Vol. **21**, p. 225; D. de Fontaine and J. Kulik, Acta Metall. **33**, 145 (1985).
[7] R. J. Elliott, Phys. Rev. **124**, 346 (1961).
[8] M. E. Fisher and W. Selke, Phys. Rev. Lett. **44**, 1502 (1980); Philos. Trans. R. Soc. London **302**, 1 (1981).
[9] J. von Boehm and P. Bak, Phys. Rev. Lett. **42**, 122 (1979); P. Bak and J. von Boehm, Phys. Rev. B **21**, 5297 (1980).
[10] O. Terasaki and D. Watanabe, Jpn. J. Appl. Phys. **20**, L381

[10]O. Terasaki and D. Watanabe, Jpn. J. Appl. Phys. **20**, L381 (1981).
[11]B. Widom, J. Chem. Phys. **84**, 6943 (1986).
[12]K. A. Dawson, Phys. Rev. A **36**, 3383 (1987).
[13]K. A. Dawson, M. D. Lipkin, and B. Widom, J. Chem. Phys. **88**, 5149 (1988).
[14]W. Selke and M. E. Fisher, Z. Phys. B **40**, 71 (1980).
[15]J. Oitmaa and M. J. Velgakis, J. Phys. A **20**, 1495 (1987).
[16]J. Oitmaa, M. T. Batchelor, and M. N. Barber, J. Phys. A **20**, 1507 (1987).
[17]P. M. Duxbury and W. Selke, J. Phys. A **16**, L741 (1983); W. Selke and P. M. Duxbury, Z. Phys. B **57**, 49 (1984).
[18]P. Upton and J. Yeomans, Europhys. Lett. **5**, 575 (1988).
[19]D. H. Lyons and T. A. Kaplan, J. Phys. Chem. Solids **25**, 645 (1964).
[20]C. Domb, Adv. Phys. **9**, 149 (1960).
[21]R. Kikuchi, Phys. Rev. **81**, 988 (1951).
[22]R. M. Hornreich, M. Luban, and S. Shtrikman, Phys. Rev. Lett. **35**, 1678 (1975); A. Michelson, Phys. Rev. B **16**, 577 (1977).
[23]G. H. Wannier, Phys. Rev. **79**, 357 (1950).